

Learning low-dimensional dynamical-system models from noisy frequency-response data with Loewner rational interpolation

Zlatko Drmač* Benjamin Peherstorfer†

November 2020

Dedicated to Athanasios C Antoulas on the occasion of his 70th birthday.

Loewner rational interpolation provides a versatile tool to learn low-dimensional dynamical-system models from frequency-response measurements. This work investigates the robustness of the Loewner approach to noise. The key finding is that if the measurements are polluted with Gaussian noise, then the error due to noise grows at most linearly with the standard deviation with high probability under certain conditions. The analysis gives insights into making the Loewner approach robust against noise via linear transformations and judicious selections of measurements. Numerical results demonstrate the linear growth of the error on benchmark examples.

Keywords: data-driven modeling; nonintrusive model reduction; interpolatory model reduction; Loewner

1 Introduction

Learning dynamical-system models from measurements is a widely studied task in science, engineering, and machine learning; see, e.g., system identification originating from the systems & control community [1, 39, 29, 27, 51, 22, 38, 40, 15, 10, 11], sparsity-promoting methods [43, 44, 8, 42], dynamic mode decomposition [46, 45, 41, 50, 24, 9], and operator inference [33, 32, 37, 23, 34, 49, 30]. Antoulas and collaborators introduced the Loewner approach [2, 25, 28, 5] that constructs models directly from frequency-response measurements, without requiring computationally expensive training phases and without solving potentially non-convex optimization problems. This work investigates the robustness of the Loewner approach to noise in the frequency-response measurements. The main finding of this work is that under certain conditions and with high probability the error introduced by noise into Loewner models grows at most linearly with the standard deviation of the noise.

The Loewner approach [2, 25, 28, 5] derives dynamical-system models from frequency-response data, i.e., from values of the transfer function of the high-dimensional dynamical system of interest. A series of works have extended the Loewner approach from linear time-invariant systems to bilinear systems [4], quadratic-bilinear systems [13], parametrized systems [18], time-delay systems [47], and structured systems [48]. Learning Loewner models from time-domain data, instead of frequency-response measurements, is discussed in [20, 31]. Learning Loewner models from noisy data has received relatively little attention.

*Faculty of Science, Department of Mathematics, University of Zagreb, Bijenička 30, 10000 Zagreb, Croatia

†Courant Institute of Mathematical Sciences, New York University, New York, NY 10012, USA

The work [26] provides a numerical investigation of the effect of noise on the accuracy of Loewner models. The work [17] discusses the rank of Hankel matrices if measurements are polluted by additive Gaussian noise. Numerical experiments in the thesis [19, Section 2.1] demonstrate that the selection of frequencies at which to obtain measurements and how to partition the measurements has a significant influence on the robustness against perturbations in the data such as noise. The work [21] applies the Loewner approach to control tasks where only noisy measurements are available. The authors of [6] discuss the robustness of interpolatory model reduction against perturbations in evaluations of the transfer function of the high-dimensional system; however, the perturbations are considered deterministic and stem from, e.g., numerical approximations via iterative methods. During the writing of this manuscript, the authors became aware of the work [12] that studies the sensitivity of Loewner interpolation to perturbations in a deterministic fashion via pseudospectra of the Loewner matrix pencils.

In this work, the robustness of the Loewner approach to Gaussian noise is considered. Rather than a deterministic analysis, the contribution of this work is an analysis that bounds the error introduced by noise in a probabilistic sense. In particular, the analysis shows that the error grows at most linearly in the standard deviation of the noise under certain conditions and with high probability. A relative noise model is considered, which seems realistic because measurement errors typically are relative to the value of the measured quantities. The conditions under which the proposed error bounds hold give insights into selecting the frequencies at which to measure and partitioning the data to reduce the effect of noise. The linear growth of the error with respect to the standard deviation of the noise is observed in numerical examples.

2 Learning low-dimensional dynamical-system models with Loewner rational interpolation

This section recapitulates model reduction with the Loewner approach; see, e.g., [3, 7, 35] for general introductions to model reduction and related concepts.

2.1 Linear time-invariant dynamical systems

Consider the linear time-invariant system

$$E\dot{x}(t) = Ax(t) + Bu(t), \quad y(t) = Cx(t) \quad (1)$$

of order $N \in \mathbb{N}$ with system matrices $E, A \in \mathbb{R}^{N \times N}$, $B \in \mathbb{R}^{N \times 1}$, and $C \in \mathbb{R}^{1 \times N}$. The state at time t is $x(t) \in \mathbb{R}^N$ and the output at time t is $y(t) \in \mathbb{R}$. The transfer function is

$$H(s) = C(sE - A)^{-1}B, \quad s \in \mathbb{C}.$$

In the following, we only consider systems with full-rank matrix E .

2.2 Loewner rational interpolation

To derive a reduced model of dimension $n \in \mathbb{N}$ of system (1), consider $2n$ interpolation points $s_1, \dots, s_{2n} \in \mathbb{C}$. The interpolation points are partitioned into two sets $\{\mu_1, \dots, \mu_n\}$ and $\{\gamma_1, \dots, \gamma_n\}$ of equal size. Define the $n \times n$ Loewner matrix L and the $n \times n$ shifted Loewner matrix $L^{(s)}$ as

$$L_{ij} = \frac{H(\mu_i) - H(\gamma_j)}{\mu_i - \gamma_j}, \quad L_{ij}^{(s)} = \frac{\mu_i H(\mu_i) - \gamma_j H(\gamma_j)}{\mu_i - \gamma_j}, \quad i, j = 1, \dots, n,$$

together with the $n \times 1$ input matrix \widehat{B} and the $1 \times n$ output matrix \widehat{C} with components

$$\widehat{B}_i = H(\mu_i), \quad \widehat{C}_i = H(\gamma_i), \quad i = 1, \dots, n. \quad (2)$$

The Loewner model is

$$\widehat{E}\dot{\hat{x}}(t) = \widehat{A}\hat{x}(t) + \widehat{B}u(t), \quad \hat{y}(t) = \widehat{C}\hat{x}(t)$$

with $\widehat{E} = -L$ and $\widehat{A} = -L^{(s)}$. The n -dimensional state at time t is $\hat{x}(t)$ and the output at time t is $\hat{y}(t)$. The transfer function of the Loewner model is

$$\widehat{H}(s) = \widehat{C}(s\widehat{E} - \widehat{A})^{-1}\widehat{B}, \quad s \in \mathbb{C}.$$

The Loewner approach guarantees that the transfer function \widehat{H} of the Loewner model interpolates the transfer function H of the system (1) at the interpolation points s_1, \dots, s_{2n} , which means

$$H(s_i) = \widehat{H}(s_i), \quad i = 1, \dots, 2n.$$

3 Learning Loewner models from noisy frequency-response measurements

We now study the robustness of the Loewner approach to noise in the transfer-function values of the system (1). The key contribution is Theorem 1 that bounds the error that is introduced by noise under certain conditions.

3.1 Noisy transfer-function values

Let $\mu \in \mathbb{C}$ with the real part $\Re(\mu)$ and the imaginary part $\Im(\mu)$ and let $0 < \sigma \in \mathbb{R}$. We denote with $\epsilon \sim \mathcal{CN}(\mu, \sigma)$ a complex random variable, where the real $\Re(\epsilon)$ and the imaginary part $\Im(\epsilon)$ are independently normally distributed. The real part $\Re(\epsilon)$ has mean $\Re(\mu)$, the imaginary part $\Im(\epsilon)$ has mean $\Im(\mu)$. The real and the imaginary part of ϵ have standard deviation σ .

Let $\epsilon_1, \dots, \epsilon_n \sim \mathcal{CN}(0, 1)$ and $\eta_1, \dots, \eta_n \sim \mathcal{CN}(0, 1)$ be independent random variables. Define the noisy transfer-function values as

$$H_\sigma(\mu_i) = H(\mu_i)(1 + \sigma\epsilon_i), \quad H_\sigma(\gamma_i) = H(\gamma_i)(1 + \sigma\eta_i), \quad i = 1, \dots, n,$$

so that

$$H_\sigma(\mu_i) \sim \mathcal{CN}(H(\mu_i), H(\mu_i)\sigma), \quad H_\sigma(\gamma_i) \sim \mathcal{CN}(H(\gamma_i), H(\gamma_i)\sigma), \quad i = 1, \dots, n.$$

The noise pollutes the transfer-function values in a relative sense, i.e., the standard deviation of $H_\sigma(\mu_i)$ is scaled by $H(\mu_i)$. We consider such a relative noise model to be realistic in our situation because measurement errors typically are relative to the value of the quantity that is measured. Note, however, that the technics used in the following analysis can be extended to an absolute noise model, where the standard deviation of the noise is independent of the transfer-function value; see Section 3.5.

3.2 Loewner and noisy transfer-function values

From the noisy transfer-function values, we derive the noisy Loewner matrices

$$\tilde{L}_{ij} = \frac{H_\sigma(\mu_i) - H_\sigma(\gamma_j)}{\mu_i - \gamma_j}, \quad \tilde{L}_{ij}^{(s)} = \frac{\mu_i H_\sigma(\mu_i) - \gamma_j H_\sigma(\gamma_j)}{\mu_i - \gamma_j}, \quad i, j = 1, \dots, n,$$

which have the same structure as in Section 2.2, except that the noisy transfer-function values $H_\sigma(\mu_1), \dots, H_\sigma(\mu_n), H_\sigma(\gamma_1), \dots, H_\sigma(\gamma_n)$ are used rather than the noiseless values $H(\mu_1), \dots, H(\mu_n), H(\gamma_1), \dots, H(\gamma_n)$. We decompose the noisy Loewner and the noisy shifted Loewner matrix into deterministic and random parts as

$$\tilde{L} = L + \sigma\delta L, \quad \tilde{L}^{(s)} = L^{(s)} + \sigma\delta L^{(s)},$$

with

$$\delta L_{ij} = \frac{H(\mu_i)\epsilon_i - H(\gamma_j)\eta_j}{\mu_i - \gamma_j}, \quad \delta L_{ij}^{(s)} = \frac{\mu_i H(\mu_i)\epsilon_i - \gamma_j H(\gamma_j)\eta_j}{\mu_i - \gamma_j}, \quad i, j = 1, \dots, n.$$

We obtain the system matrices

$$\tilde{E} = \hat{E} + \sigma \delta E, \quad \tilde{A} = \hat{A} + \sigma \delta A,$$

where $\delta E = -\delta L_{ij}$ and $\delta A = -\delta L_{ij}^{(s)}$. Similarly, we define $\tilde{B} = \hat{B} + \sigma \delta B$ and $\tilde{C} = \hat{C} + \sigma \delta C$ with

$$\delta B_i = H(\mu_i)\epsilon_i, \quad \delta C_i = H(\gamma_i)\eta_i, \quad i = 1, \dots, n. \quad (3)$$

The Loewner model learned from the noisy transfer-function values is then given by

$$\tilde{E}\dot{\tilde{x}}(t) = \tilde{A}\tilde{x}(t) + \tilde{B}u(t), \quad \tilde{y}(t) = \tilde{C}\tilde{x}(t), \quad (4)$$

with the n -dimensional state $\tilde{x}(t)$ at time t and the output $\tilde{y}(t)$ at time t . The transfer function of the model (4) is

$$\tilde{H}(s) = \tilde{C}(s\tilde{E} - \tilde{A})^{-1}\tilde{B}, \quad s \in \mathbb{C}.$$

We call (4) the noisy Loewner model.

3.3 Noise structure

The Loewner and the shifted Loewner matrices introduce a structure in the noise that is added to the system matrices of the Loewner model learned from the noisy transfer-function values. Consider the matrix $s\delta E - \delta A$ and obtain

$$\begin{aligned} s\delta E_{ij} - \delta A_{ij} &= -\frac{1}{\mu_i - \gamma_j} (sH(\mu_i)\epsilon_i - sH(\gamma_j)\eta_j - \mu_i H(\mu_i)\epsilon_i + \gamma_j H(\gamma_j)\eta_j) \\ &= \frac{1}{\gamma_j - \mu_i} ((s - \mu_i)H(\mu_i)\epsilon_i + (-s + \gamma_j)H(\gamma_j)\eta_j) \end{aligned}$$

to write in matrix form as

$$s\delta E - \delta A = \underbrace{\begin{bmatrix} \epsilon_1 & & & \\ & \epsilon_2 & & \\ & & \ddots & \\ & & & \epsilon_n \end{bmatrix}}_{\boldsymbol{\epsilon}} + \underbrace{\begin{bmatrix} H(\mu_1)\frac{s-\mu_1}{\gamma_1-\mu_1} & \dots & H(\mu_1)\frac{s-\mu_1}{\gamma_1-\mu_n} \\ \vdots & \ddots & \vdots \\ H(\mu_n)\frac{s-\mu_n}{\gamma_1-\mu_1} & \dots & H(\mu_n)\frac{s-\mu_n}{\gamma_n-\mu_n} \end{bmatrix}}_{F_E} + \underbrace{\begin{bmatrix} H(\gamma_1)\frac{\gamma_1-s}{\gamma_1-\mu_1} & \dots & H(\gamma_n)\frac{\gamma_n-s}{\gamma_1-\mu_n} \\ \vdots & \ddots & \vdots \\ H(\gamma_1)\frac{\gamma_1-s}{\gamma_1-\mu_1} & \dots & H(\gamma_n)\frac{\gamma_n-s}{\gamma_n-\mu_n} \end{bmatrix}}_{F_A} \underbrace{\begin{bmatrix} \eta_1 & & & \\ & \eta_2 & & \\ & & \ddots & \\ & & & \eta_n \end{bmatrix}}_{\boldsymbol{\eta}}. \quad (5)$$

Equation (5) reveals that the random parts of $s\delta E - \delta A$ can be singled out into the two diagonal random matrices $\boldsymbol{\epsilon}$ and $\boldsymbol{\eta}$ of dimension $n \times n$. The diagonal entries of $\boldsymbol{\epsilon}$ and $\boldsymbol{\eta}$ are independent and have distribution $\mathcal{CN}(0, 1)$.

3.4 Bounding the error due to noisy transfer-function values

The task is to bound

$$\widehat{H}(s) - \widetilde{H}(s) = \widehat{C}(s\widehat{E} - \widehat{A})^{-1}\widehat{B} - \widetilde{C}(s\widetilde{E} - \widetilde{A})^{-1}\widetilde{B}, \quad (6)$$

where s typically takes the values in some specified $\Omega \subset \mathbb{C}$; for instance on the imaginary axis, possibly within a specified frequency range. In any case, we assume in the following that Ω is free of the poles of \widehat{H} . The following main results hold pointwise and therefore are agnostic to additional structure imposed by Ω besides that it excludes poles of \widehat{H} .

If $\widehat{\lambda}_i, \widetilde{\lambda}_i$ ($\widehat{\lambda}_i, \widetilde{\lambda}_i$) are the poles with the corresponding residues of \widehat{H} (\widetilde{H}), then [14, Proposition 3.3] gives

$$\|\widehat{H} - \widetilde{H}\|_{\mathcal{H}_2}^2 = \sum_{i=1}^n \widehat{\phi}_i(\widehat{H}(-\widehat{\lambda}_i) - \widetilde{H}(-\widehat{\lambda}_i)) + \sum_{j=1}^n \widetilde{\phi}_j(\widetilde{H}(-\widetilde{\lambda}_j) - \widehat{H}(-\widetilde{\lambda}_j)), \quad (7)$$

which shows that the error (6) is of particular interest at the reflected poles of both systems (for (7) to hold, both \widehat{H} and \widetilde{H} are assumed stable, of the same order n , and all poles of both systems are assumed simple). We do not tackle the issue of a probabilistic error bound for the \mathcal{H}_2 norm; this topic is left for our future work.

For an estimate of the error (6), we need to understand the effect of the random noise in the matrices $\widetilde{E} = \widehat{E} + \sigma\delta E$, $\widetilde{A} = \widehat{A} + \sigma\delta A$, $\widetilde{B} = \widehat{B} + \sigma\delta B$ to the solution of the linear system $(s\widetilde{E} - \widetilde{A})^{-1}\widetilde{B}$. To that end, we first briefly review the (deterministic) error bound for a solution of the perturbed system. The key is the condition number $\kappa_2(s\widehat{E} - \widehat{A}) = \|(s\widehat{E} - \widehat{A})^{-1}\|_2 \|s\widehat{E} - \widehat{A}\|_2$, see, e.g., [16, Theorem 7.2].

Proposition 1. Let s be different from the poles of \widehat{H} , and consider the perturbations (5) and (3) deterministic and bounded as $\|\sigma(s\delta E - \delta A)\|_2 \leq \zeta \|s\widehat{E} - \widehat{A}\|_2$, $\|\sigma\delta B\|_2 \leq \zeta \|\widehat{B}\|_2$, where $\zeta > 0$ is such that $\zeta\kappa_2(s\widehat{E} - \widehat{A}) < 1$. Then $s\widetilde{E} - \widetilde{A}$ is nonsingular and

$$\frac{\|(s\widetilde{E} - \widetilde{A})^{-1}\widetilde{B} - (s\widehat{E} - \widehat{A})^{-1}\widehat{B}\|_2}{\|(s\widehat{E} - \widehat{A})^{-1}\widehat{B}\|_2} \leq \frac{2\zeta}{1 - \zeta\kappa_2(s\widehat{E} - \widehat{A})} \kappa_2(s\widehat{E} - \widehat{A}). \quad (8)$$

This is the standard perturbation bound for the linear system $\widehat{G}\widehat{x} = \widehat{B}$, $\widehat{G} = s\widehat{E} - \widehat{A}$, under the deterministic perturbations $\Delta\widehat{G} = \sigma(s\delta E - \delta A)$ and $\Delta\widehat{B} = \sigma\delta B$.

Recall that by (5), $s\delta E - \delta A = \epsilon F_E + F_A \boldsymbol{\eta}$, where ϵ and $\boldsymbol{\eta}$ are diagonal matrices whose diagonals are random vectors. These can be bounded in a probabilistic sense, using concentration inequalities which we briefly review next.

Proposition 2. Let $Z = [z_1, \dots, z_n]^T$ be a random vector with independent standard normal real components $z_i \sim \mathcal{N}(0, 1)$, $i = 1, \dots, n$. Then with probability at least $1 - \exp(-n/2)$

$$\|Z\|_2 \leq 2\sqrt{n}. \quad (9)$$

If $Z = [z_1, \dots, z_n]^T$ is a vector of independent complex random variables $z_i \sim \mathcal{CN}(0, 1)$, with \mathcal{CN} defined in Section 3.1, then

$$\|Z\|_2 \leq 4\sqrt{n} \quad (10)$$

holds with probability at least $1 - 2\exp(-n/2)$.

The estimate (9) follows from Gaussian concentration and because the χ^2 distribution is sub-Gaussian; see, e.g., [52, Example 2.28]. The statement (10) follows from (9), because $\|Z\|_2 \leq \|\Re(Z)\|_2 + \|\Im(Z)\|_2$, where $\Re(Z)$ is the vector that has as components the real parts of the components of Z and $\Im(Z)$ is the vector that has as components the imaginary parts of Z .

Lemma 1. Let $s \in \Omega$, i.e., s is different from the poles of \hat{H} , be such that

$$0 < \sigma < \frac{1}{\kappa_2(s\hat{E} - \hat{A})} \min \left\{ \frac{\|s\hat{E} - \hat{A}\|_2}{4\sqrt{n}(\|F_E\|_2 + \|F_A\|_2)}, \frac{\|\hat{B}\|_2}{4\sqrt{n}\|\hat{B}\|_\infty} \right\}. \quad (11)$$

Then, with probability at least $1 - 4\exp(-n/2)$, s is not a pole of \tilde{H} and the error bound (8) in Proposition 1 holds.

Proof. Since, by (5), $s\delta E - \delta A = \epsilon F_E + F_A \boldsymbol{\eta}$, we have

$$\|s\delta E - \delta A\|_2 \leq \|\epsilon\|_2 \|F_E\|_2 + \|F_A\|_2 \|\boldsymbol{\eta}\|_2. \quad (12)$$

Because ϵ is diagonal¹ with the elements $\epsilon_1, \dots, \epsilon_n$ on the diagonal, we obtain, using Proposition 2, that

$$\|\epsilon\|_2 = \max_{i=1, \dots, n} |\epsilon_i| = \|[\epsilon_1, \dots, \epsilon_n]^T\|_\infty \leq \|[\epsilon_1, \dots, \epsilon_n]^T\|_2 \leq 4\sqrt{n}, \quad (13)$$

with probability at least $1 - 2\exp(-n/2)$. Let δB_i denote the i -th component of δB , then $\delta B_i = H(\mu_i)\epsilon_i = \hat{B}_i \epsilon_i$ holds for $i = 1, \dots, n$ and thus equation (13) means that

$$\|\delta B\|_2 \leq \|\hat{B}\|_\infty \|[\epsilon_1, \dots, \epsilon_n]^T\|_2 \leq 4\sqrt{n} \|\hat{B}\|_\infty \quad (14)$$

$$\|\tilde{B}\|_2 \leq (1 + \sigma 4\sqrt{n}) \|\hat{B}\|_2 \quad (15)$$

holds with probability at least $1 - 2\exp(-n/2)$. Similar arguments show that

$$\|\boldsymbol{\eta}\|_2 \leq 4\sqrt{n} \quad (16)$$

and

$$\|\delta C\|_2 \leq 4\sqrt{n} \|\hat{C}\|_\infty \quad (17)$$

hold with probability at least $1 - 2\exp(-n/2)$, where we used $\delta C_i = H(\gamma_i)\eta_i = \hat{C}_i \eta_i$ for $i = 1, \dots, n$. Set now

$$\zeta = \sigma \hat{\zeta}, \quad \hat{\zeta} = \max \left\{ \frac{4\sqrt{n}(\|F_E\|_2 + \|F_A\|_2)}{\|s\hat{E} - \hat{A}\|_2}, \frac{4\sqrt{n}\|\hat{B}\|_\infty}{\|\hat{B}\|_2} \right\} \quad (18)$$

and observe that (11) guarantees $\zeta \kappa_2(s\hat{E} - \hat{A}) < 1$. Thus, together with (12), it follows that

$$\begin{aligned} \|\sigma(s\delta E - \delta A)\|_2 &\leq \sigma 4\sqrt{n}(\|F_E\|_2 + \|F_A\|_2) \\ &= \sigma \frac{4\sqrt{n}(\|F_E\|_2 + \|F_A\|_2)}{\|s\hat{E} - \hat{A}\|_2} \|s\hat{E} - \hat{A}\|_2 \leq \zeta \|s\hat{E} - \hat{A}\|_2 \end{aligned} \quad (19)$$

with probability at least $(1 - 2\exp(-n/2))^2 \geq 1 - 4\exp(-n/2)$, where we used (18).

With (14) and the definition of ζ in (18), we also obtain that

$$\|\sigma \delta B\|_2 \leq \sigma 4\sqrt{n} \|\hat{B}\|_\infty = \sigma \frac{4\sqrt{n} \|\hat{B}\|_\infty}{\|\hat{B}\|_2} \|\hat{B}\|_2 \leq \zeta \|\hat{B}\|_2 \quad (20)$$

holds with probability at least $1 - 4\exp(-n/2)$. Thus, with (19), (20), and because (11) implies $\zeta \kappa_2(s\hat{E} - \hat{A}) < 1$, the error bound (8) is applicable with probability at least $1 - 4\exp(-n/2)$, which also means that $s\tilde{E} - \tilde{A}$ is nonsingular. \square

¹Note that ϵ is a diagonal *matrix* defined in (5).

The following theorem bounds the error due to noise in the transfer-function values.

Theorem 1. *Under the same assumptions as Lemma 1, for each $s \in \Omega$, there exists a constant $C_s > 0$ that may depend on s such that*

$$|\tilde{H}(s) - \hat{H}(s)| \leq C_s \sigma \quad (21)$$

holds with probability at least $1 - 4 \exp(-n/2)$.

Proof. Consider now

$$\begin{aligned} \hat{H}(s) - \tilde{H}(s) &= \hat{C}(s\hat{E} - \hat{A})^{-1}\hat{B} - \tilde{C}(s\tilde{E} - \tilde{A})^{-1}\tilde{B} \\ &= \hat{C} \left((s\hat{E} - \hat{A})^{-1}\hat{B} - (s\tilde{E} - \tilde{A})^{-1}\tilde{B} \right) - \sigma\delta C(s\tilde{E} - \tilde{A})^{-1}\tilde{B} \end{aligned}$$

and take the absolute value to obtain

$$|\hat{H}(s) - \tilde{H}(s)| \leq c_1 \frac{\zeta}{1 - \zeta\kappa_2(s\hat{E} - \hat{A})} + |\sigma\delta C(s\tilde{E} - \tilde{A})^{-1}\tilde{B}|, \quad (22)$$

where we invoked (8) with

$$c_1 = 2\|\hat{C}\|_2 \|(s\hat{E} - \hat{A})^{-1}\hat{B}\|_2 \kappa_2(s\hat{E} - \hat{A}) \quad (23)$$

and ζ set as in (18). Note that (8) holds with probability at least $1 - 4 \exp(-n/2)$, and thus (22) holds with the same probability.

We now bound $\|(s\tilde{E} - \tilde{A})^{-1}\|_2$ in probability. Consider the Neumann expansion

$$\begin{aligned} (s\tilde{E} - \tilde{A})^{-1} &= \left(s\hat{E} - \hat{A} + \sigma(s\delta E - \delta A) \right)^{-1} \\ &= (s\hat{E} - \hat{A})^{-1} \sum_{i=0}^{\infty} (-1)^i \sigma^i \left((s\delta E - \delta A)(s\hat{E} - \hat{A})^{-1} \right)^i, \quad (24) \end{aligned}$$

where the series converges to the inverse of $I + \sigma(s\delta E - \delta A)(s\hat{E} - \hat{A})^{-1}$ provided that² $\|\sigma(s\delta E - \delta A)(s\hat{E} - \hat{A})^{-1}\|_2 < 1$. Because (19) holds with probability at least $1 - 4 \exp(-n/2)$, we obtain that with the same probability of at least $1 - 4 \exp(-n/2)$

$$\|\sigma(s\delta E - \delta A)(s\hat{E} - \hat{A})^{-1}\|_2 \leq \zeta \|s\hat{E} - \hat{A}\|_2 \|(s\hat{E} - \hat{A})^{-1}\|_2 < 1,$$

holds, where we used assumption (11) in the second inequality. Note that the second inequality is strict. Set

$$\nu = 4\sqrt{n}(\|F_E\|_2 + \|F_A\|_2) \|(s\hat{E} - \hat{A})^{-1}\|_2,$$

and obtain with (19), (24), and $\sigma\nu < 1$ because of (11) that

$$\|(s\tilde{E} - \tilde{A})^{-1}\|_2 \leq \|(s\hat{E} - \hat{A})^{-1}\|_2 \sum_{i=0}^{\infty} (\nu\sigma)^i = \|(s\hat{E} - \hat{A})^{-1}\|_2 \frac{1}{1 - \nu\sigma} \quad (25)$$

holds with probability at least $1 - 4 \exp(-n/2)$.

Then, we obtain the bound

$$\begin{aligned} |\sigma\delta C(s\tilde{E} - \tilde{A})^{-1}\tilde{B}| &\leq \sigma\|\delta C\|_2 \|(s\tilde{E} - \tilde{A})^{-1}\|_2 \|\tilde{B}\|_2 \\ &\leq 4\sqrt{n}\|\hat{C}\|_{\infty} \|\hat{B}\|_2 \|(s\hat{E} - \hat{A})^{-1}\|_2 \frac{\sigma(1 + \sigma 4\sqrt{n})}{1 - \nu\sigma} \\ &\leq c_2 \frac{\sigma + \sigma^2 4\sqrt{n}}{1 - \nu\sigma}, \quad (26) \end{aligned}$$

²The necessary and sufficient condition for the convergence is that the spectral radius of $\sigma(s\delta E - \delta A)(s\hat{E} - \hat{A})^{-1}$ is strictly less than one.

where we used (15), (17) and (25), which together hold with probability at least $1 - 4 \exp(-n/2)$, and we set $c_2 = 4\sqrt{n}\|\widehat{C}\|_\infty\|\widehat{B}\|_2\|(s\widehat{E} - \widehat{A})^{-1}\|_2$.

We obtain with (22), (26) the following bound

$$|\widehat{H}(s) - \widetilde{H}(s)| \leq \sigma \left[\frac{c_1 \widehat{\zeta}}{1 - \sigma \widehat{\zeta} \kappa_2(s\widehat{E} - \widehat{A})} + \frac{c_2(1 + \sigma 4\sqrt{n})}{1 - \nu\sigma} \right], \quad (27)$$

which grows at most linearly in σ as long as condition (11) is satisfied, which shows (21). \square

Corollary 1. *Under the same conditions as Theorem 1 and for $s \in \Omega$ that are not zeros of \widehat{H} ,*

$$\frac{|\widetilde{H}(s) - \widehat{H}(s)|}{|\widehat{H}(s)|} \leq C_s \sigma \quad (28)$$

holds with probability at least $1 - 4 \exp(-n/2)$ and constant $C_s > 0$ that may depend on s .

Proof. Note that $\widehat{H}(s)$ is independent of σ and thus dividing (21) by $|\widehat{H}(s)|$ is sufficient to show (28) if s is not a zero of \widehat{H} . To highlight a geometric interpretation of (28), we show (28) via a different approach. Since $|\widehat{H}(s)| = \|\widehat{C}\|_2\|(s\widehat{E} - \widehat{A})^{-1}\widehat{B}\|_2 |\cos \angle(\widehat{C}^*, (s\widehat{E} - \widehat{A})^{-1}\widehat{B})|$, the factor c_1 defined in (23) can be interpreted as

$$c_1 = |\widehat{H}(s)| \frac{2\kappa_2(s\widehat{E} - \widehat{A})}{|\cos \angle(\widehat{C}^*, (s\widehat{E} - \widehat{A})^{-1}\widehat{B})|}$$

so that the first term on the right-hand side in (27) contains the bound on the relative error $|\widehat{H}(s) - \widetilde{H}(s)|/|\widehat{H}(s)|$ with the two natural condition numbers $\kappa_s(s\widehat{E} - \widehat{A})$ and $|\cos \angle(\widehat{C}^*, (s\widehat{E} - \widehat{A})^{-1}\widehat{B})|$. The interpretation is as follows: Evaluating \widetilde{H} essentially means solving a perturbed linear system $(s\widetilde{E} - \widetilde{A})^{-1}\widetilde{B}$ and then computing an inner product $(\widetilde{C}^*)^*((s\widetilde{E} - \widetilde{A})^{-1}\widetilde{B})$ with a perturbed vector \widetilde{C}^* . The sensitivity of the solution of a system of equations to perturbations is quantified by the condition number $\kappa_2(s\widehat{E} - \widehat{A})$ and the sensitivity of the inner product is quantified by $|\cos \angle(\widehat{C}^*, (s\widehat{E} - \widehat{A})^{-1}\widehat{B})|$. Similarly, the second term on the right-hand side in (27) can be modified as follows: Instead of (26), estimate the second term in (22) as

$$\begin{aligned} |\sigma \delta C (s\widetilde{E} - \widetilde{A})^{-1}\widetilde{B}| &\leq \sigma 4\sqrt{n}\|\widehat{C}\|_\infty\|(s\widehat{E} - \widehat{A})^{-1}\widehat{B}\|_2 \left(1 + \frac{2\zeta\kappa_2(s\widehat{E} - \widehat{A})}{1 - \zeta\kappa_2(s\widehat{E} - \widehat{A})} \right) \\ &= \sigma |\widehat{H}(s)| \frac{4\sqrt{n}}{|\cos \angle(\widehat{C}^*, (s\widehat{E} - \widehat{A})^{-1}\widehat{B})|} \frac{1 + \zeta\kappa_2(s\widehat{E} - \widehat{A})}{1 - \zeta\kappa_2(s\widehat{E} - \widehat{A})} \frac{\|\widehat{C}\|_\infty}{\|\widehat{C}\|_2}. \end{aligned}$$

Hence, because $\widehat{H}(s) \neq 0$ per assumption, we can write

$$\frac{|\widehat{H}(s) - \widetilde{H}(s)|}{|\widehat{H}(s)|} \leq \sigma \left(\frac{1}{|\cos \vartheta_s|} \left(\frac{2\widehat{\zeta}\kappa_2^{(s)}}{1 - \sigma\widehat{\zeta}\kappa_2^{(s)}} + 4\sqrt{n} \frac{1 + \zeta\kappa_2^{(s)}}{1 - \zeta\kappa_2^{(s)}} \frac{\|\widehat{C}\|_\infty}{\|\widehat{C}\|_2} \right) \right) \quad (29)$$

where $\vartheta_s = \angle(\widehat{C}^*, (s\widehat{E} - \widehat{A})^{-1}\widehat{B})$ and $\kappa_2^{(s)} = \kappa_2(s\widehat{E} - \widehat{A})$. \square

3.5 Remarks on Theorem 1

The following remarks are in order. First, note that condition (11) implies that $\widetilde{H}(s)$ exists with probability at least $1 - 4 \exp(-n/2)$. Second, a similar result as in Theorem 1 can be shown for an absolute noise model, i.e., where the noisy transfer-function values $\widetilde{H}(s)$ have a standard deviation that is independent of the transfer-function value $H(s)$. The major change is that matrices F_A and F_E defined in (5) are independent

of the transfer-function values when an absolute noise model is used and thus condition (11) holds for a different range of standard deviations σ than for a relative noise model. Third, condition (11) in Theorem 1 depends on the scaling of the entries of the system matrices \hat{E} , \hat{A} , \hat{B} , and \hat{C} . Consider two nonsingular matrices D_1 and D_2 of size $n \times n$. Then, the Loewner model given by \hat{E} , \hat{A} , \hat{B} , \hat{C} , derived from noiseless transfer-function values, can be transformed as

$$\check{E} = D_1 \hat{E} D_2, \quad \check{A} = D_1 \hat{A} D_2, \quad \check{B} = D_1 \hat{B}, \quad \check{C} = \hat{C} D_2,$$

with transfer function $\check{H}(s) = \check{C}(s\check{E} - \check{A})^{-1}\check{B}$. It holds $\check{H}(s) = \hat{H}(s)$ for $s \in \mathbb{C}$; however, the condition number $\kappa_2(s\hat{E} - \hat{A})$ is *not* invariant under the transformation given by D_1 and D_2 , which means that condition (11) in Theorem 1 is not invariant if the system is transformed. A component-wise analysis [16, Section 7.2] could be an option to derive a version of Theorem 1 that is invariant under diagonal linear transformations D_1 and D_2 . Fourth, condition (11) in Theorem 1 depends on the interpolation points s_1, \dots, s_{2n} and on the partition $\{\mu_1, \dots, \mu_n\}, \{\gamma_1, \dots, \gamma_n\}$, which shows that the interpolation points and their partition can influence the robustness of the Loewner approach to noise; cf., e.g., [19, Section 2.1]. Our numerical results demonstrate that different choices of interpolation points indeed influence condition (11) and thus when the linear growth of the error (21) with the standard deviation σ of the noise holds. The numerical results below suggest that taking interpolation points that keep the condition number of $s\hat{E} - \hat{A}$ low seems reasonable. However, additional analyses and numerical experiments are necessary before one can give a definitive recommendation. The issue of selection and partition of the interpolation points is an important challenging problem that will be addressed in our future work.

4 Numerical results

In this section, we demonstrate the error bound of Theorem 1 on numerical experiments with some well known benchmark examples.

4.1 CD player

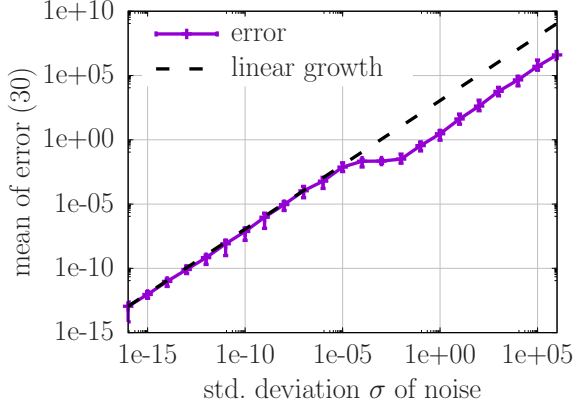
The system of a CD player is a common benchmark problem for model reduction and can be downloaded from the SLICOT website ³.

4.1.1 Problem setup

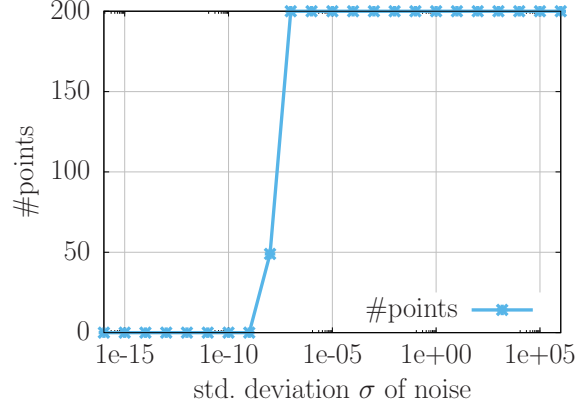
We consider single-input-single-output (SISO) systems and therefore we use only the first input and the second output of the CD-player system. The frequency range is $[2\pi, 200\pi]$, which contains some of the major dynamics of the CD-player system. The order of the system is $N = 120$. To derive a Loewner model of order n , we select $2n$ interpolation points as follows. First, n points w_1, \dots, w_n are selected logarithmically equidistant in the range $[2\pi, 200\pi]$ on the imaginary axis. Then, $s_i = (-1)^i w_i$ for $i = 1, \dots, n$ and $s_{n+i} = (-1)^{i+1} w_i$. The first n points s_1, \dots, s_n are put into the set $\{\mu_1, \dots, \mu_n\}$ and the following n points s_{n+1}, \dots, s_{2n} are put into $\{\gamma_1, \dots, \gamma_n\}$. To test the Loewner models, we select 200 test points $s_1^{\text{test}}, \dots, s_{200}^{\text{test}}$ on the imaginary axis in the range $[2\pi, 200\pi]$.

From the noiseless transfer-function values $H(\mu_1), \dots, H(\mu_n)$ and $H(\gamma_1), \dots, H(\gamma_n)$ a Loewner model is derived with transfer function \hat{H} . Then, the transfer-function values are polluted with noise with standard deviation σ as described in Section 3.1 and a noisy Loewner model is derived with transfer function \tilde{H}_σ . Note that we now explicitly denote standard deviation as subscript in the transfer functions of noisy Loewner models.

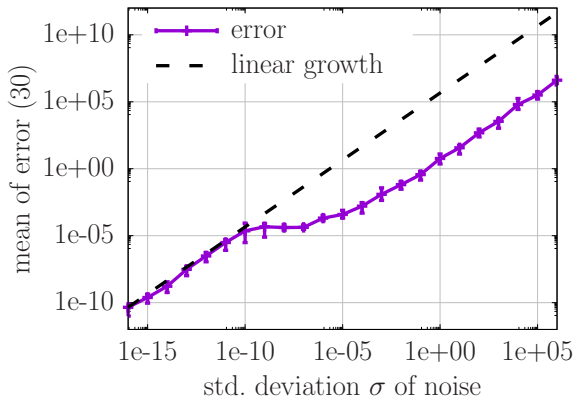
³<http://slicot.org/20-site/126-benchmark-examples-for-model-reduction>



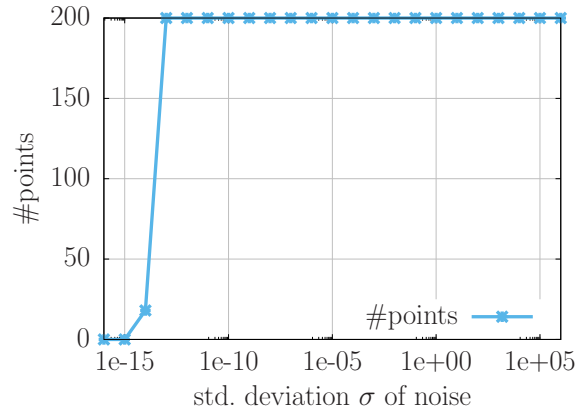
(a) error, dimension $n = 20$



(b) assumption (11) violated, dimension $n = 20$



(c) error, dimension $n = 28$



(d) assumption (11) violated, dimension $n = 28$

Figure 1: CD player: Plots (a) and (c) show the growth of the mean of error (30) over 10 replicates of independent noise samples. Plots (b) and (d) show the number of test points for which condition (11) of Theorem 1 is violated. The mean of the error (30) grows linearly with σ as long as condition (11) is satisfied, which is in agreement with Theorem 1. The error bars in (a) and (c) show the minimum and maximum of the error (30) over the 10 replicates of the noise samples.

4.1.2 Results

We consider the error

$$e(\sigma) = \frac{1}{200} \sum_{i=1}^{200} |\hat{H}(s_i^{\text{test}}) - \tilde{H}_\sigma(s_i^{\text{test}})|, \quad (30)$$

which is an average of the error (21) over all 200 test points. Figure 1a shows the mean of $e(\sigma)$ over 10 replicates of independent noise samples. The standard deviation σ is in the range $[10^{-15}, 10^5]$ and the dimension is $n = 20$. The error bars in Figure 1a show the minimum and maximum of $e(\sigma)$ over the 10 replicates. A linear growth of the mean of error (30) with the standard deviation σ is observed for $\sigma < 10^{-5}$. Figure 1b shows the number of test points that violate condition (11) of Theorem 1. The results indicate that for $\sigma \geq 10^{-7}$ condition (11) is violated for all 200 test points, which seems to align with Figure 1a that shows a linear growth for $\sigma < 10^{-5}$. Thus, the results in Figure 1a are in agreement with Theorem 1. Similar observations can be made for $n = 28$ in Figure 1c and Figure 1d.

4.2 Penzl

The Penzl system is a benchmark problem that has been introduced in [36, Example 3] and is used in, e.g., [19, 31] to demonstrate the Loewner approach.

4.2.1 Problem setup

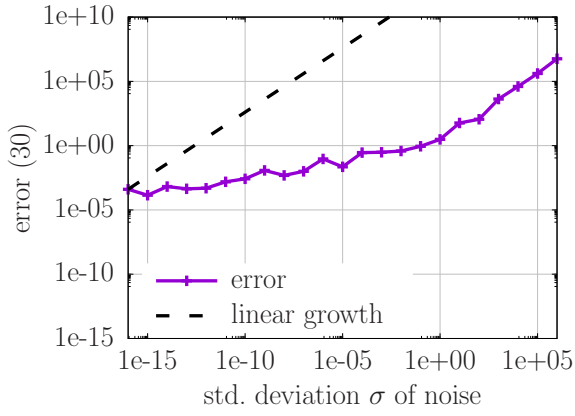
The Penzl system is of order $N = 1006$ and we consider the frequency range $[10, 1000]$. We consider two different sets of interpolation points in this example. First, we select n logarithmically equidistant points on the imaginary axis in the range $[10, 1000]$ and include their complex conjugates as described in Section 4.1.1. We denote the corresponding set of $2n$ interpolation points as \mathcal{E}_n . Second, we select points randomly in the imaginary plane in the range $[10, 1000] \times \iota[10, 1000]$, where ι is the complex unit $\iota = \sqrt{-1}$. To select the points randomly, we first select 10^6 logarithmically equidistant points w_1, \dots, w_{10^6} in $[10, 1000]$ and then draw uniformly $2n$ points from w_1, \dots, w_{10^6} for the real and imaginary parts of the n interpolation points s_1, \dots, s_n . Then, their complex conjugates are $s_{n+i} = \bar{s}_i$ for $i = 1, \dots, n$. The interpolation points are partitioned into the two sets $\{\mu_1, \dots, \mu_n\}$ and $\{\gamma_1, \dots, \gamma_n\}$ with $\mu_i = s_{2i-1}$ and $\gamma_i = s_{2i}$ for $i = 1, \dots, n$ such that complex pairs are in the same set. The set of interpolation points is denoted as \mathcal{R}_n . The test points are 200 points selected on the imaginary axis in the range $[10, 1000]$.

4.2.2 Results

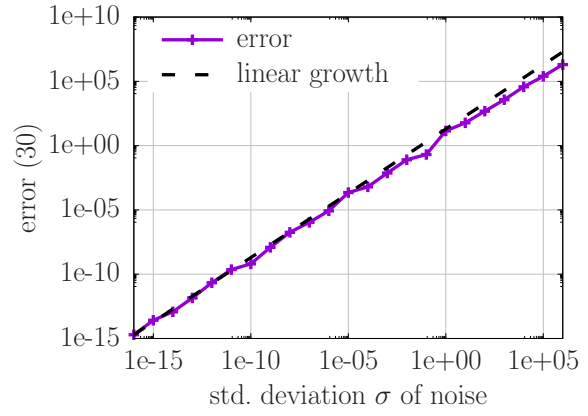
Figure 2a shows the error (30) corresponding to the Loewner model with interpolation points \mathcal{R}_n (random) and of dimension $n = 16$. Figure 2c shows that condition (11) is violated for all test points and all standard deviations σ in the range $[10^{-15}, 10^5]$, which means that Theorem 1 is not applicable. In contrast, Figure 2b shows a linear growth for the error (30) corresponding to the models learned from logarithmically equidistant points \mathcal{E}_n . Figure 2d indicates that up to $\sigma = 10^{-10}$ the condition (11) for Theorem 1 is satisfied, which explains the linear growth for $\sigma \leq 10^{-10}$. For $\sigma > 10^{-10}$, Theorem 1 is not applicable, even though a linear growth is observed, which demonstrates that Theorem 1 is rather pessimistic in this example. Figure 3 shows the magnitude of the transfer functions for $\sigma = 10^{-6}$ and demonstrates that the logarithmically equidistant points \mathcal{E}_n seem to provide more robustness against noise than the random points \mathcal{R}_n in this example. The numerical observations seem to be in alignment with Theorem 1 because assumption (11) is violated for interpolation points \mathcal{R}_n for all σ considered in Figure 2c, whereas assumption (11) is satisfied for small σ for points \mathcal{E}_n . Note that the condition number of $s\hat{E} - \hat{A}$ plays a critical role in the assumption (11). Thus, it seems that taking interpolation points that keep the condition number of $s\hat{E} - \hat{A}$ low is reasonable. However, additional analyses and numerical experiments are necessary before one can give a definitive recommendation.

Acknowledgements

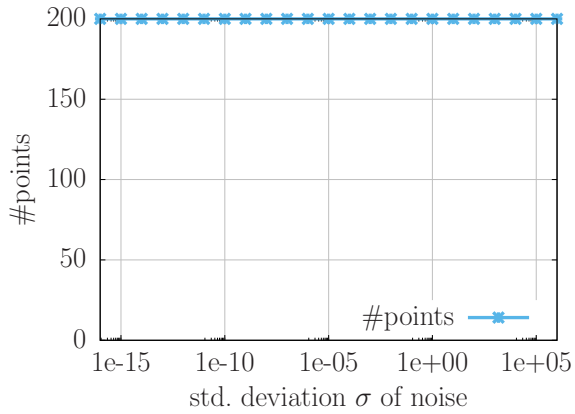
Drmač was supported in parts by the DARPA Contract HR0011-18-9-0033, the ONR Contract N00014-19-C-1053, and the Croatian Science Foundation through Grant IP-2019-04-6268 “*Randomized low rank algorithms and applications to parameter dependent problems.*” Peherstorfer was partially supported by US Department of Energy, Office of Advanced Scientific Computing Research, Applied Mathematics Program (Program Manager Dr. Steven Lee), DOE Award DESC0019334 and by the National Science Foundation under Grant No. 1901091. The numerical experiments were computed with support through the NYU IT High Performance Computing resources, services, and staff expertise.



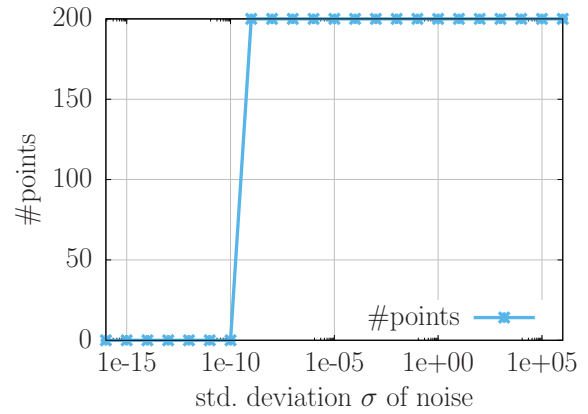
(a) error, interpolation points \mathcal{R}_n



(b) error, interpolation points \mathcal{E}_n

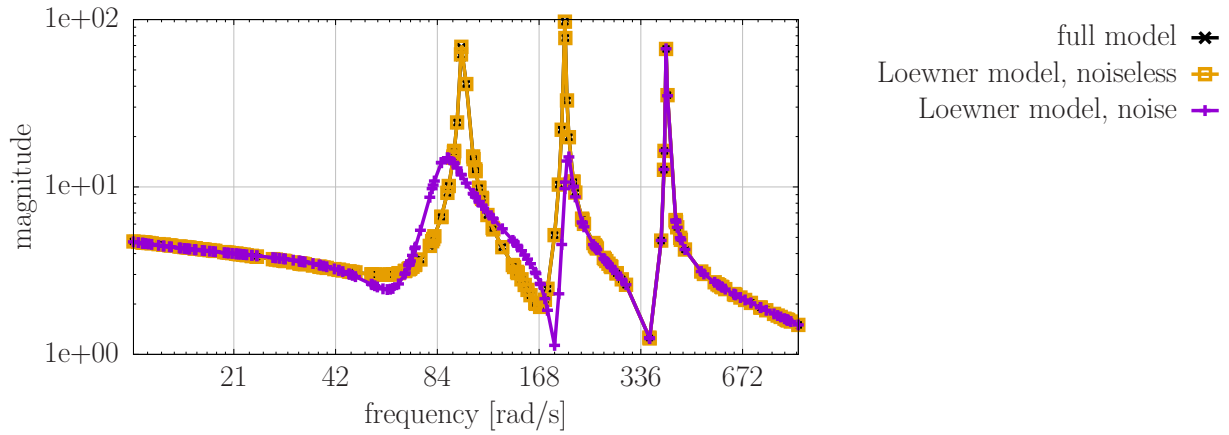


(c) assumption (11), interpolation points \mathcal{R}_n

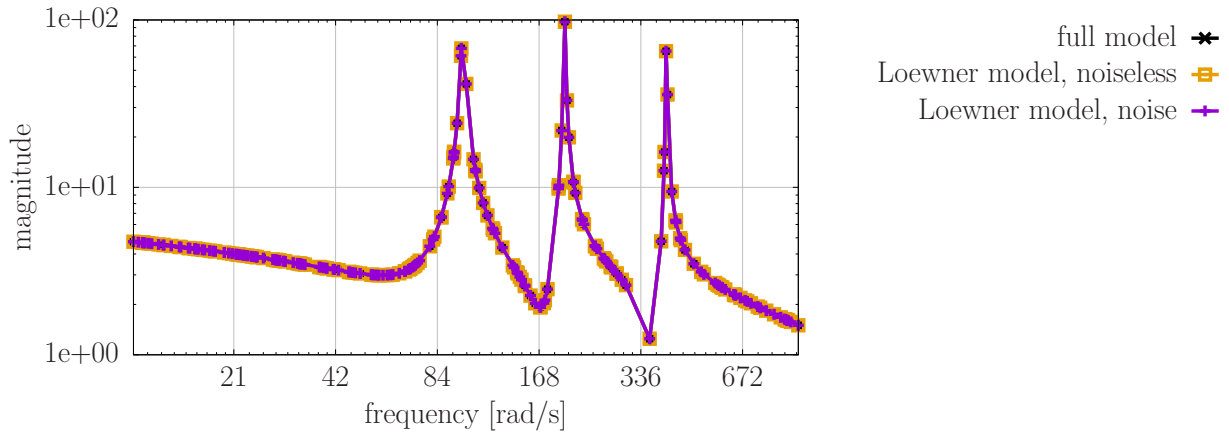


(d) assumption (11), interpolation points \mathcal{E}_n

Figure 2: Penzl: The choice of the interpolation points can have a significant effect on the robustness of the Loewner approach to noise. Plots (a) and (c) show results for points selected randomly and plots (b) and (d) for points selected logarithmically equidistantly. Learning Loewner models from the logarithmically equidistant points seems to be more robust in this example than learning from the randomly selected points.



(a) Models learned from randomly selected points



(b) Models learned from logarithmically equidistant points

Figure 3: Penzl: Plots (a) and (b) show the magnitude of the transfer function of Loewner models learned from noiseless transfer-function values and from transfer-function values polluted with noise with standard deviation $\sigma = 10^{-6}$. The interpolation points are randomly selected in (a) and logarithmically equidistant in (b); compare with Figure 2.

References

- [1] K. Abderrahim, H. Mathlouthi, and F. Msahli. New approaches to finite impulse response systems identification using higher-order statistics. *IET Signal Processing*, 4(5):488–501, 2010.
- [2] A. Antoulas and B. D. O. Anderson. On the scalar rational interpolation problem. *IMA Journal of Mathematical Control & Information*, 3(2-3):61–88, 1986.
- [3] A. Antoulas, C. Beattie, and S. Gugercin. Interpolatory model reduction of large-scale dynamical systems. In J. Mohammadpour and K. Grigoriadis, editors, *Efficient Modeling and Control of Large-Scale Systems*. Springer-Verlag, 2010.
- [4] A. Antoulas, I. Gosea, and A. Ionita. Model reduction of bilinear systems in the Loewner framework. *SIAM Journal on Scientific Computing*, 38(5):B889–B916, 2016.
- [5] C. Beattie and S. Gugercin. Realization-independent \mathcal{H}_2 -approximation. In *Proc. IEEE Conf. Decis. Control*, pages 4953–4958, Maui, HI, USA, 2012.
- [6] C. Beattie, S. Gugercin, and S. Wyatt. Inexact solves in interpolatory model reduction. *Linear Algebra and its Applications*, 436(8):2916 – 2943, 2012. Special Issue dedicated to Danny Sorensen’s 65th birthday.
- [7] P. Benner, S. Gugercin, and K. Willcox. A survey of projection-based model reduction methods for parametric dynamical systems. *SIAM Review*, 57(4):483–531, 2015.
- [8] S. L. Brunton, J. L. Proctor, and J. N. Kutz. Discovering governing equations from data by sparse identification of nonlinear dynamical systems. *Proceedings of the National Academy of Sciences*, 113(15):3932–3937, 2016.
- [9] Z. Drmač, I. Mezić, and R. Mohr. Data driven modal decompositions: analysis and enhancements. *SIAM Journal on Scientific Computing*, 40(4):A2253–A2285, 2018.
- [10] Z. Drmač, S. Gugercin, and C. Beattie. Quadrature-based vector fitting for discretized \mathcal{H}_2 approximation. *SIAM Journal on Scientific Computing*, 37(2):A625–A652, 2015.
- [11] Z. Drmač, S. Gugercin, and C. Beattie. Vector fitting for matrix-valued rational approximation. *SIAM Journal on Scientific Computing*, 37(5):A2346–A2379, 2015.
- [12] M. Embree and A. C. Ionita. Pseudospectra of Loewner matrix pencils. *arXiv:1910.12153*, pages 1–18, 2019.
- [13] I. V. Gosea and A. C. Antoulas. Data-driven model order reduction of quadratic-bilinear systems. *Numerical Linear Algebra with Applications*, 25(6):e2200, 2018.
- [14] S. Gugercin, A. Antoulas, and C. Beattie. \mathcal{H}_2 model reduction for large-scale linear dynamical systems. *SIAM Journal on Matrix Analysis and Applications*, 30(2):609–638, Jan. 2008.
- [15] B. Gustavsen and A. Semlyen. Rational approximation of frequency domain responses by vector fitting. *Power Delivery, IEEE Transactions on*, 14(3):1052–1061, Jul 1999.
- [16] N. J. Higham. *Accuracy and Stability of Numerical Algorithms*. SIAM, 2002.
- [17] J. M. Hokanson. A data-driven McMillan degree lower bound. *SIAM Journal on Scientific Computing*, 42(5):A3447–A3461, 2020.
- [18] A. Ionita and A. Antoulas. Data-driven parametrized model reduction in the Loewner framework. *SIAM Journal on Scientific Computing*, 36(3):A984–A1007, 2014.

- [19] A. C. Ionita. *Lagrange rational interpolation and its applications to approximation of large-scale dynamical systems*. PhD thesis, Rice University, 2013.
- [20] A. C. Ionita and A. C. Antoulas. *Matrix pencils in time and frequency domain system identification*, pages 79–88. Control, Robotics and Sensors. Institution of Engineering and Technology, 2012.
- [21] P. Kergus, S. Formentin, C. Poussot-Vassal, and F. Demourant. Data-driven control design in the Loewner framework: Dealing with stability and noise. In *2018 European Control Conference (ECC)*, pages 1704–1709, June 2018.
- [22] B. Kramer and S. Gugercin. Tangential interpolation-based eigensystem realization algorithm for MIMO systems. *Mathematical and Computer Modelling of Dynamical Systems*, 22(4):282–306, 2016.
- [23] B. Kramer, B. Peherstorfer, and K. Willcox. Feedback control for systems with uncertain parameters using online-adaptive reduced models. *SIAM Journal on Applied Dynamical Systems*, 16(3):1563–1586, 2017.
- [24] J. N. Kutz, S. L. Brunton, B. W. Brunton, and J. L. Proctor. *Dynamic mode decomposition: Data-driven modeling of complex systems*. SIAM, 2016.
- [25] S. Lefteriu and A. Antoulas. A new approach to modeling multiport systems from frequency-domain data. *Computer-Aided Design of Integrated Circuits and Systems, IEEE Transactions on*, 29(1):14–27, Jan 2010.
- [26] S. Lefteriu, A. C. Ionita, and A. C. Antoulas. Modeling systems based on noisy frequency and time domain measurements. In J. C. Willems, S. Hara, Y. Ohta, and H. Fujioka, editors, *Perspectives in Mathematical System Theory, Control, and Signal Processing: A Festschrift in Honor of Yutaka Yamamoto on the Occasion of his 60th Birthday*, pages 365–378, Berlin, Heidelberg, 2010. Springer Berlin Heidelberg.
- [27] L. Ljung. *System identification*. Prentice Hall, 1987.
- [28] A. Mayo and A. Antoulas. A framework for the solution of the generalized realization problem. *Linear Algebra and its Applications*, 425(2-3):634 – 662, 2007.
- [29] J. Mendel. Tutorial on higher-order statistics (spectra) in signal processing and system theory: theoretical results and some applications. *Proc. IEEE*, 79:278–305, 1991.
- [30] B. Peherstorfer. Sampling low-dimensional Markovian dynamics for preasymptotically recovering reduced models from data with operator inference. *SIAM Journal on Scientific Computing*, 42(5):A3489–A3515, 2020.
- [31] B. Peherstorfer, S. Gugercin, and K. Willcox. Data-driven reduced model construction with time-domain Loewner models. *SIAM Journal on Scientific Computing*, 39(5):A2152–A2178, 2017.
- [32] B. Peherstorfer and K. Willcox. Dynamic data-driven reduced-order models. *Computer Methods in Applied Mechanics and Engineering*, 291:21–41, 2015.
- [33] B. Peherstorfer and K. Willcox. Data-driven operator inference for nonintrusive projection-based model reduction. *Computer Methods in Applied Mechanics and Engineering*, 306:196–215, 2016.
- [34] B. Peherstorfer and K. Willcox. Dynamic data-driven model reduction: Adapting reduced models from incomplete data. *Advanced Modeling and Simulation in Engineering Sciences*, 3(11), 2016.
- [35] B. Peherstorfer, K. Willcox, and M. Gunzburger. Survey of multifidelity methods in uncertainty propagation, inference, and optimization. *SIAM Review*, 60(3):550–591, 2018.

- [36] T. Penzl. Algorithms for model reduction of large dynamical systems. *Linear Algebra and its Applications*, 415(2-3):322 – 343, 2006.
- [37] E. Qian, B. Kramer, A. N. Marques, and K. E. Willcox. Transform & learn: A data-driven approach to nonlinear model reduction. In *AIAA Aviation 2019 Forum*, 2019.
- [38] S. J. Qin. An overview of subspace identification. *Computers & Chemical Engineering*, 30(10-12):1502 – 1513, 2006.
- [39] L. Rabiner, R. Crochiere, and J. Allen. FIR system modeling and identification in the presence of noise and with band-limited inputs. *IEEE Transactions on Acoustics, Speech, and Signal Processing*, 26(4):319–333, 1978.
- [40] E. Reynders. System identification methods for (operational) modal analysis: Review and comparison. *Archives of Computational Methods in Engineering*, 19(1):51–124, 2012.
- [41] C. Rowley, I. Mezić, S. Bagheri, P. Schlatter, and D. Henningson. Spectral analysis of nonlinear flows. *Journal of Fluid Mechanics*, 641:115–127, 12 2009.
- [42] S. H. Rudy, S. L. Brunton, J. L. Proctor, and J. N. Kutz. Data-driven discovery of partial differential equations. *Science Advances*, 3(4), 2017.
- [43] H. Schaeffer, R. Caffisch, C. D. Hauck, and S. Osher. Sparse dynamics for partial differential equations. *Proceedings of the National Academy of Sciences*, 110(17):6634–6639, 2013.
- [44] H. Schaeffer, G. Tran, and R. Ward. Extracting sparse high-dimensional dynamics from limited data. *SIAM Journal on Applied Mathematics*, 78(6):3279–3295, 2018.
- [45] P. Schmid. Dynamic mode decomposition of numerical and experimental data. *Journal of Fluid Mechanics*, 656:5–28, 8 2010.
- [46] P. Schmid and J. Sesterhenn. Dynamic mode decomposition of numerical and experimental data. In *Bull. Amer. Phys. Soc., 61st APS meeting*, page 208. American Physical Society, 2008.
- [47] P. Schulze and B. Unger. Data-driven interpolation of dynamical systems with delay. *Systems & Control Letters*, 97:125 – 131, 2016.
- [48] P. Schulze, B. Unger, C. Beattie, and S. Gugercin. Data-driven structured realization. *Linear Algebra and its Applications*, 537:250 – 286, 2018.
- [49] R. Swischuk, B. Kramer, C. Huang, and K. Willcox. Learning physics-based reduced-order models for a single-injector combustion process. *AIAA Journal*, 58(6):2658–2672, 2020.
- [50] J. H. Tu, C. W. Rowley, D. M. Luchtenburg, S. L. Brunton, and J. N. Kutz. On dynamic mode decomposition: Theory and applications. *Journal of Computational Dynamics*, 1(2):391–421, 2014.
- [51] M. Viberg. Subspace-based methods for the identification of linear time-invariant systems. *Automatica*, 31(12):1835 – 1851, 1995. Trends in System Identification.
- [52] M. J. Wainwright. *High-Dimensional Statistics: A Non-Asymptotic Viewpoint*. Cambridge Series in Statistical and Probabilistic Mathematics. Cambridge University Press, 2019.